INTERFACE FOCUS

royalsocietypublishing.org/journal/rsfs

Research

Cite this article: Hatala KG, Gatesy SM, Falkingham PL. 2021 Integration of biplanar X-ray, three-dimensional animation and particle simulation reveals details of human 'track ontogeny'. *Interface Focus* **11**: 20200075. https://doi.org/10.1098/rsfs.2020.0075

Accepted: 16 June 2021

One contribution of 12 to a theme issue 'Biological anthroengineering'.

Subject Areas:
biomechanics

Keywords:
palaeoanthropology, footprints, trace fossils, discrete element method, X-ray Reconstruction of Moving Morphology (XROMM)

Author for correspondence:
Kevin G. Hatala
e-mail: kevin.g.hatala@gmail.com

Electronic supplementary material is available online at https://doi.org/10.6084/m9.figshare.c.5486374.

THE ROYAL SOCIETY PUBLISHING

Integration of biplanar X-ray, three-dimensional animation and particle simulation reveals details of human 'track ontogeny'

Kevin G. Hatala[1], Stephen M. Gatesy[2] and Peter L. Falkingham[3]

[1]Department of Biology, Chatham University, Pittsburgh, PA 15232, USA
[2]Department of Ecology and Evolutionary Biology, Brown University, Providence, RI 02912, USA
[3]School of Biological and Environmental Sciences, Liverpool John Moores University, Liverpool L3 3AF, UK

KGH, 0000-0001-9131-5304; SMG, 0000-0003-1701-0320; PLF, 0000-0003-1856-8377

The emergence of bipedalism had profound effects on human evolutionary history, but the evolution of locomotor patterns within the hominin clade remains poorly understood. Fossil tracks record *in vivo* behaviours of extinct hominins, and they offer great potential to reveal locomotor patterns at various times and places across the human fossil record. However, there is no consensus on how to interpret anatomical or biomechanical patterns from tracks due to limited knowledge of the complex foot–substrate interactions through which they are produced. Here, we implement engineering-based methods to understand human track formation with the ultimate goal of unlocking invaluable information on hominin locomotion from fossil tracks. We first developed biplanar X-ray and three-dimensional animation techniques that permit visualization of subsurface foot motion as tracks are produced, and that allow for direct comparisons of foot kinematics to final track morphology. We then applied the discrete element method to accurately simulate the process of human track formation, allowing for direct study of human track ontogeny. This window lets us observe how specific anatomical and/or kinematic variables shape human track morphology, and it offers a new avenue for robust hypothesis testing in order to infer patterns of foot anatomy and motion from fossil hominin tracks.

1. Introduction

Central to the study of human evolution are questions concerning the evolution of our unique form of bipedal locomotion. While bipedalism has long been considered a defining trait of the hominin clade [1], discoveries within the past half-century have made it apparent that multiple forms of bipedalism likely existed among fossil hominins. Some of these forms were probably quite similar to our own bipedal locomotion but others were almost certainly quite different [2]. To date, most evidence for the inferred locomotor patterns of fossil hominins has come from comparative morphological studies of postcranial skeletal fossils. However, fossil hominin tracks (i.e. footprints) have augmented, and have the potential to further augment, these comparative osteological studies in important ways.

Tracks offer the only *in vivo* data on whole-foot anatomy, foot posture and foot kinematics in fossil hominins. Fossil hominin foot bones are most often found in isolation and even the most exceptional, 'nearly complete' hominin foot skeletons are missing important elements (e.g. OH 8 (*Homo habilis* [3]); LB1 (*Homo floresiensis* [4]); Foot 1 (*Homo naledi* [5]); DIK-1-1f (*Australopithecus afarensis* [6])). Tracks are sedimentological features that result from the dynamic interaction between the composite foot morphology (articulated foot skeleton and its soft tissues) and a deformable substrate. Understanding or reverse-engineering this interaction means tracks can offer a picture of extinct hominin

foot morphology complementary to that offered by the bones alone. At the same time, tracks record aspects of the three-dimensional (3D) kinematics of feet as they navigated deformable substrates [7], allowing one to observe the sequence of foot postures and motion patterns that were actually used during bouts of terrestrial bipedalism that are recorded on track surfaces. While the articular surfaces of skeletal fossils might provide rough estimates of maximal joint mobility (but see [8]), tracks result from specific poses and motion sequences that can help one to understand how hominin feet were actually used to accomplish particular forms of bipedal locomotion.

In addition to tracks being able to augment analyses of skeletal fossils in critical ways, fossil hominin track sites have been discovered at a high rate in recent years. The known record of hominin track sites that predate modern humans has experienced notable growth [9–15]. In some cases, the sample sizes of hominin tracks now exceed by more than an order of magnitude the sample of hominin foot skeletal fossils from the same time periods [12]. New technologies are also being applied to digitally record hominin tracks in 3D, thereby opening doors for digital preservation, data sharing and computational analyses [16,17].

Yet despite the great potential of these data and numerous recent advances in hominin ichnology, there still exist major obstacles that limit access to the invaluable information preserved by fossil hominin tracks. Perhaps the most important obstacle is our currently limited understanding of the complex interactions between foot anatomy, kinematics and substrate through which a track is formed [18–20]. Morse *et al*. [21] demonstrated, through a case study of Holocene human tracks from Namibia, that track morphology can vary substantially as the same individual walks through substrates of different consistencies. Yet the underlying reasons for that variation remain unknown. Deciphering the mechanical nature of foot–substrate interactions is essential for linking aspects of track morphology to anatomical or kinematic patterns [19] and thereby for leveraging hominin tracks to better understand the evolution of human foot anatomy and locomotion.

Falkingham & Gatesy [22] coined the term 'track ontogeny' to describe the mechanical process through which tracks are formed. This term emphasizes the fact that track features arise and transform through a dynamic sequence of continuous interactions between foot and substrate within each step. Differences in these interactions are responsible for variation among tracks made by the same individual. Unfortunately, this developmental sequence is inherently difficult to study because track creation is usually hidden from view—both human feet and natural substrates are opaque and so their interactions cannot be observed directly. Building upon earlier biomechanical and robotic studies that used X-rays to visualize subsurface motion (e.g. [23]), Ellis & Gatesy [24] and Falkingham & Gatesy [22] introduced biplanar X-ray approaches for studying 3D foot–substrate interactions that result in track formation. Those studies focused on track formation in guineafowl, but their biplanar X-ray approach was more recently adapted and applied to study track formation in humans [25].

Falkingham & Gatesy [22] were also the first to use particle simulation to understand track ontogeny, by using the discrete element method (DEM) to examine the mechanistic origins of track morphology. The DEM simulates individual sediment particles as they interact with each other and external geometry. These particle interactions are governed by physical parameters including elasticity, compressibility, cohesion and mass [26,27]. By iteratively simulating track formation processes, with consistent validation using experimental data, Falkingham & Gatesy [22] and Falkingham *et al*. [28] were able to leverage their ontogenetic perspective to develop robust inferences of trackmaker foot anatomy and foot kinematics from fossil dinosaur tracks.

Here, we present the development and first application of similar methods that employ biplanar X-ray, 3D animation and particle simulation to study track ontogeny in humans walking through deformable muds. We build on existing methods in important ways, most notably by animating and simulating high-resolution deformable 3D models of human feet as they interact with deformable substrates. We present a case study in which we demonstrate the application of new methods, and potential directions for future research. These methods allow us to open the black box of the foot–substrate interactions through which tracks are formed, and they provide an avenue for robust inferences of foot anatomy and kinematic patterns to be derived from fossil hominin tracks.

2. Methods

2.1. Biplanar X-ray experiments

2.1.1. Subjects

The methods presented here were developed and applied through experiments that are part of a broader study, which includes a larger subject pool. As a proof of the methodological concepts, we present here focused analyses from only one individual. Subjects were recruited and provided informed consent to participate through protocols approved by the Institutional Review Boards of Chatham University and Brown University.

2.1.2. Biplanar X-ray set-up and technique

The biplanar X-ray equipment, and its configuration within the W.M. Keck Foundation XROMM (X-ray Reconstruction of Moving Morphology) Facility at Brown University closely followed that used previously by Hatala *et al*. [25]. Details on this configuration and recording settings are provided in the electronic supplementary material, text S1.

2.1.3. Trackway and substrates

A roughly 6 m long (approx. 60 cm wide, approx. 50 cm tall) elevated trackway was assembled, following a set-up that we have used previously to study human track formation via biplanar X-ray [25]. The biplanar X-ray apparatus was configured at roughly the centre of this trackway, with the two X-ray beams at an angle of approximately 90° to each other. To improve the visibility of markers on the sole of the foot, the X-ray beams were pitched upwards 10° relative to the ground plane. X-ray emitters and image intensifiers were placed with a source-to-image distance of 134 cm. X-ray videos captured anteromedial and anterolateral projections of each subject's right foot.

The trackway was configured such that different substrates of interest could be placed within the area of biplanar X-ray overlap. A modified stone slab table formed a rigid and stable base within this central portion of the trackway. Three rigid, closed-cell extruded polystyrene (EPS) foam panels (two 5 cm thick, one 2.5 cm thick) were placed on top of the stone slab, and a diamond-shaped recess was cut in the centre of them, providing a space in which an interchangeable substrate container could be securely placed (figure 1).

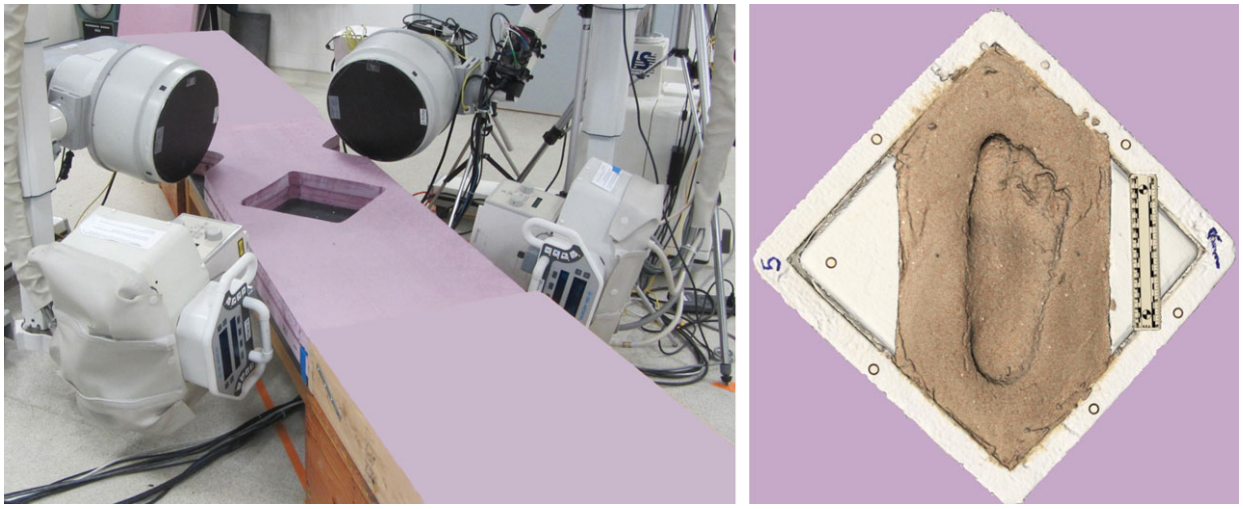

Figure 1. Edited photo showing trackway and biplanar X-ray configuration used in track formation experiments. Portions of the trackway preceding and following the central, substrate-bearing section were covered with various foams to make the entire trackway level and equally deformable under each substrate condition. The central section includes a diamond-shaped recess into which substrate containers were placed. The panel on the right shows an overhead view of a 3D scan of the substrate container, with a track produced within it (in 'hydrated 5' mud).

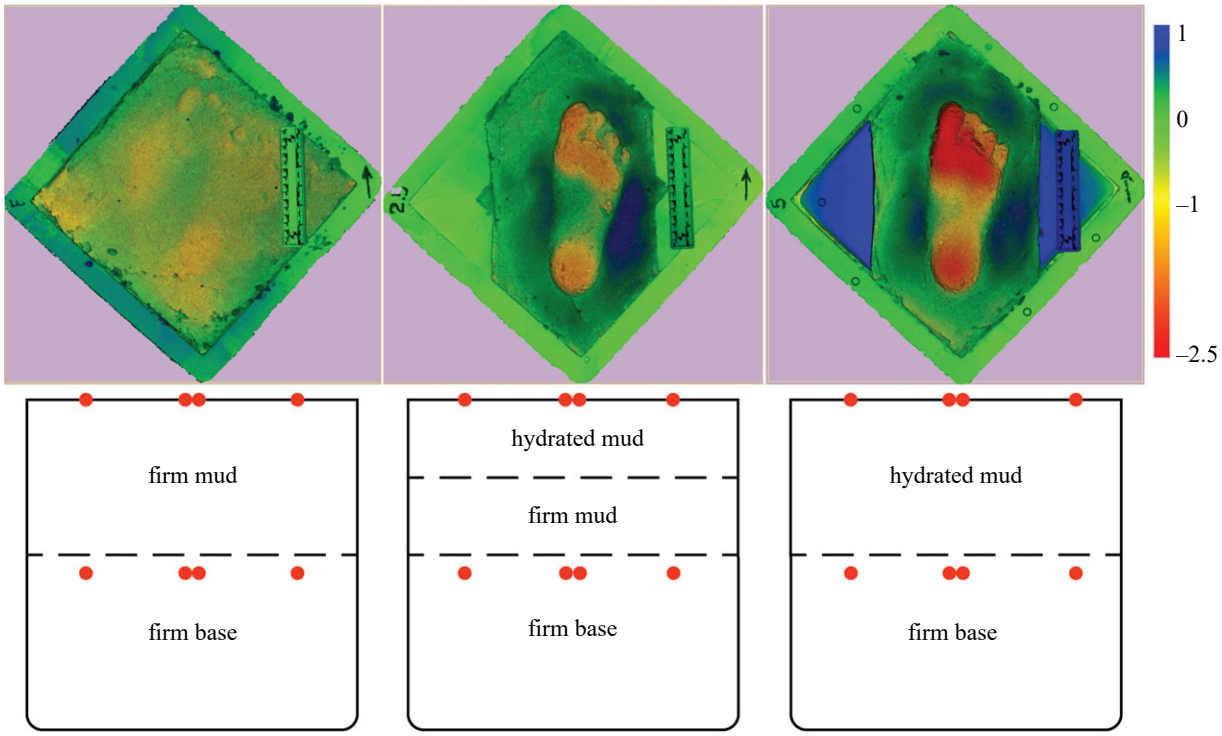

Figure 2. Side-by-side comparisons of 3D track models from the same subject in the three varieties of mud (top row), alongside schematics showing the contents of substrate containers (bottom row). Substrates included 'firm' mud (left), 'hydrated 2.5' mud (centre) and 'hydrated 5' mud (right). Track depth is reflected by colour gradients according to the scale at the far right, which is displayed in centimetres. Each substrate container included 6.5 cm of 'firm base', and an overlying 5 cm that was filled according to the substrate conditions of that particular trial. At the locations of red dots, radiopaque marker beads were placed within and upon each substrate in diamond-shaped patterns, to align the final track model within the same calibrated space as the foot during 3D animation.

This configuration allowed for the study of foot motion on four substrates. In one set-up, a rigid foam core carbon fibre panel (79 × 30.5 × 2.7 cm) was placed over the top of the recess, and 2.5 cm closed-cell EPS foam panels were placed along the remaining length of the trackway in order to make it level. In the remaining three set-ups, a square foam container (30 × 30 cm opening, 14.5 cm deep, with 3 cm walls) was placed within the recess. Foam wedges were placed in the medial and lateral corners of the substrate container, in order to reduce the volume of 'unnecessary' mud that X-rays would have to traverse but that would not interact with the foot (thereby improving the clarity of the X-ray videos). This left an area 22 cm wide, which held one of three varieties of mud into which the foot would impress (figure 2). In these configurations, the remainder of the trackway was topped with panels of rigid, closed-cell EPS foam (for 'firm' mud, described below) or soft, deformable upholstery foams (approx. 2.5 cm thick for 'hydrated 2.5' mud, 5 cm thick for 'hydrated 5' mud, described below) to mimic the deformative natures of the substrates of interest and provide a level surface along the entire trackway length.

Building upon previous biplanar X-ray studies of track formation [22,25,29], we developed a new range of radiolucent,

deformable and cohesive substrates that mimic the mechanical behaviours and particle dimensions of naturally occurring sediments. These substrates consisted of 60 µm glass bubbles (Type K15; 3M Co., St. Paul, MN, USA), modelling clay, water and acrylic blast media (Type V, 0.42–0.56 mm diameter; Kramer Industries, Inc., Piscataway, NJ, USA). The first three ingredients were mixed in a 24 : 5 : 9 volumetric ratio (following [29]) and this combination was then mixed with the acrylic blast media in roughly equal volumetric proportions. In filling the substrate containers, a substantial base portion would not interact directly with the subjects' feet. In the bottom-most 6.5 cm of the substrate, we integrated EPS foam pellets (2–4 mm diameter; LACrafts) with the above ingredients, to further enhance radiolucency while still maintaining relatively consistent material properties throughout the substrate volume. Slightly beneath the surface of this firm base, we placed three or four radiopaque markers 3 mm in diameter, such that we could track those points and identify and account for any potential disturbance to the entire substrate volume. The remaining 5 cm were then filled with one of three substrate variants. In the 'firm' condition, the container was filled to the rim with substrate and tightly packed by tamping with a rubber mallet. In the 'hydrated 2.5' condition, 2.5 cm of 'firm' substrate was added atop the firm base. Water was added to the substrate to make it more fluid and deformable and this filled the most superficial 2.5 cm of the container. In the 'hydrated 5' condition, the entire most superficial 5 cm of the container was filled with the hydrated substrate. On the surface of each of these substrates, we again placed four radiopaque beads 3 mm in diameter, such that we could use those points to register the position of the final track during 3D animation (figure 2).

2.1.4. Experimental protocol

Subjects had an array of 85 radiopaque beads placed on the external surface of their right foot, the motions of which could be tracked via biplanar X-ray. Some of these markers were placed at anatomical locations of interest, but others filled in gaps to provide a roughly uniform mesh of markers across the entire plantar surface of the foot. This array of bead markers expands upon a 70-marker array used in earlier experiments [25] to achieve even more complete surface coverage. Before marker beads were placed, a template was drawn on each subject's foot using semi-permanent marker. The foot was then 3D scanned using a handheld structured light scanner (Creaform Go!SCAN 50; Creaform, Lévis, Québec, Canada; figure 3). Following scanning of the foot with its marker template, 1.5 mm diameter radiopaque markers (SureMark, Simi Valley, CA, USA) were placed and secured using medical adhesive (SkinTac; Torbot, Cranston, RI, USA). These markers are small enough that they are hardly palpable between the foot and substrate, and subjects reported no discomfort or interference with their normal patterns of walking. After markers were placed, subjects moved to the experimental trackway and walked across it several times until they were fully comfortable moving within that environment.

Subjects traversed the experimental trackway for at least 13 trials each. In one trial, the subjects simply stood with their right foot on the carbon fibre plate (with their left foot immediately behind for support) while a single pair of X-ray images were taken of their 'statically loaded' marked foot. Each subject then walked across each of the four substrates (carbon fibre and the three mud variants) for at least three trials at their self-selected comfortable walking speed. If their foot strayed outside of the biplanar X-ray volume, they were asked to repeat that trial. For trials in which subjects walked through mud, the track they created was 3D scanned. For most trials, the structured light scanner was used to scan the track, with the scanner set to capture data continuously at 1.0 mm resolution (true resolution is sub-millimetre). However, there were nine trials in which the scanning

Figure 3. High-resolution 3D scan of a subject's foot with template for marker placements drawn in semi-permanent marker. Views are plantar (centre), lateral (left), medial (right) and dorsal (top). No markers were placed on the dorsum of the foot aside from those on the dorsal sides of the toes.

software was still processing the model from the previous trial, and therefore we scanned tracks using photogrammetry (Canon 5D Mark III camera; Canon, Melville, NY, USA; Agisoft Metashape Professional v. 1.6.4; Agisoft LLC, St. Petersburg, Russia). Photogrammetric models were also acquired with sub-millimetre resolution. After track scanning, the surface beads were removed, the substrate was relevelled using a trowel, and new surface beads put in place. Following three successful recordings, the container was swapped for a different substrate before the next trial.

2.2. Motion tracking and 3D animations

XMALab software (v. 1.5.5) was used to compute the 3D trajectories of radiopaque marker beads that were placed on the foot, as it moved on and within the substrates of interest. Following protocols that were established for XROMM [30,31], XMALab was used to remove distortion from video recordings, calibrate the 3D volume in which biplanar X-rays overlapped, and then track marker trajectories in 3D. Since our markers were placed on non-rigid human feet, and we sought to track soft tissue deformations and motions, there was no informed basis for applying a filter to these data. Further, we used XMALab's polynomial fitting procedure to improve sub-pixel accuracy (a procedure that has been shown to reduce standard deviations of inter-marker distances on rigid bodies [31]), and recorded at speeds of only 50 Hz, which should have the effect of minimizing potential 'noise' in 3D marker trajectories. Additional details regarding marker tracking are provided in the electronic supplementary material, text S2.

High-resolution scans of subjects' feet were processed and cleaned using Creaform VXElements software (v. 7.0.1). Built-in mesh editing features were used to remove noisy polygons (i.e. those discontinuous with the foot model) and to trim the foot model such that it included, in general, only the area distal to the medial and lateral malleoli. These 3D models were exported in .obj format and then imported in Autodesk Maya 2020 for animation.

In the animation protocol, the high-resolution foot mesh was first imported to Autodesk Maya 2020. For each individual trial, the 3D coordinates of foot markers were imported into Maya and animated as a collection of spheres each 1.5 mm in diameter using the 'imp' function of XROMM MayaTools (v. 2.2.3) [32]. The positions of these spheres were linked to the positions of the bead markers on the surface of the high-resolution foot model (figure 3; electronic supplementary material, text S3).

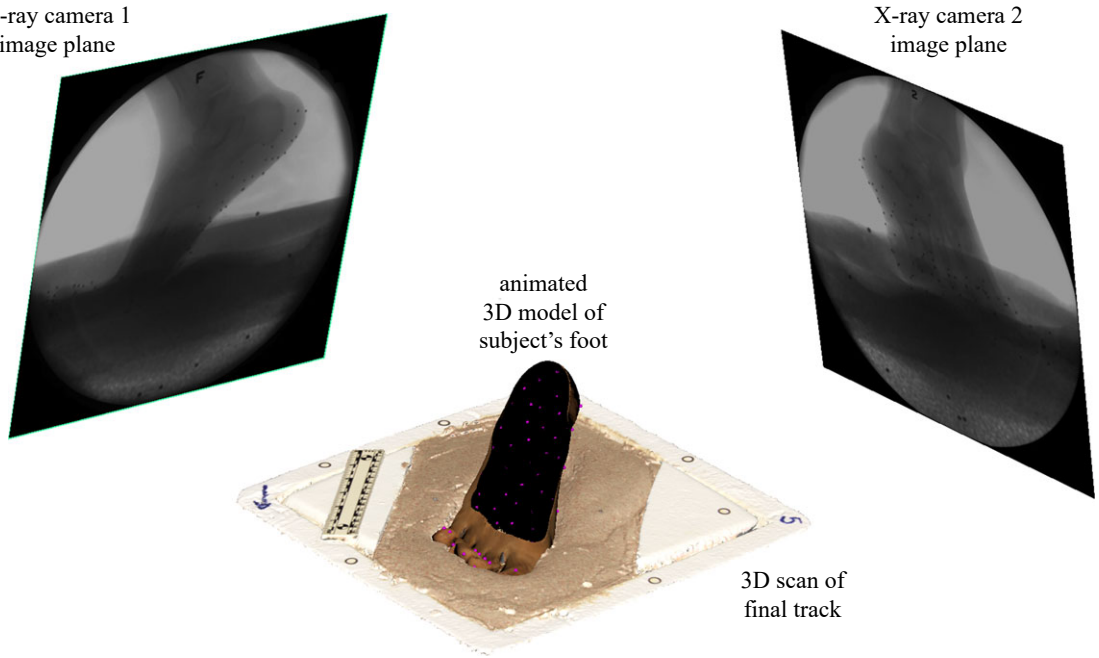

Figure 4. Snapshot of an animation of a single trial from biplanar X-ray experiments. The position of the mobile and deformable high-resolution 3D foot scan is continuously guided by the tracked 3D positions of external foot markers. Markers on the external surface of the foot appear as black dots in X-ray camera views and are highlighted in purple for the sake of visibility on the animated foot model. The foot animation is integrated with a 3D model of the final track that was produced in this trial, registered within the same calibrated 3D space. Integration of feet and tracks within the same animation scene allows for direct visualization of the correspondence between track morphology and pedal kinematics.

The spheres were interconnected such that their motions moved the vertices of a low-resolution mesh, which in turn drove motions of the high-resolution mesh using Maya's wrap deformer function (electronic supplementary material, text S3 and figure S1). Through this series of connections and deformations, biplanar X-ray data were used to create trial- and subject-specific animations of both aerial and subsurface skin movements during track formation (figure 4).

Spheres (3.0 mm in diameter) were also animated to represent markers placed within and upon the substrate (figure 2). The final configuration of the four markers visible on the tracked surface were used to translate and rotate the scan- or photogrammetry-derived 3D track model into registration. Such registration is critical for assessing the correspondence (or lack of correspondence) between pedal kinematics and track morphology. However, because only the final track was captured, the integration of a dynamic foot with a static footprint (figure 4) is insufficient to fully explain the origin and modification of specific features during a step. For insights into the interplay between foot shape, foot motion and substrate displacement, we turned to simulation.

2.3. Simulating track formation

We used LIGGGHTS (www.cfdem.com; [27]) to carry out discrete element simulations of foot–substrate interactions. Our simulation process began with relatively simple foot motions and iteratively increased motion complexity, culminating in the deforming foot animation. All simulations used the same initial particle set-up and parameters. A virtual tray 21 × 35 cm and 8 cm deep was created in Autodesk Maya in the same world-space position as the original substrate container. This completely encompassed the track-forming volume, though the virtual tray lacked the diamond-shaped ends of the real substrate container for computational simplicity. The virtual tray was filled with approximately 800 000 particles of 2 mm diameter. While this particle size is homogeneous and significantly larger than the experimental substrate, particle properties (Young modulus, Poisson ratio, cohesion and friction) were adjusted such that the macroscopic bulk behaviour was similar to that of our substrate. Simulations were carried out in the same world-space as the biplanar X-ray experiments, so simulated and real tracks could be directly compared without requiring manual or automated registration.

The simplest simulation involved a vertical stamping of a rigid foot model (the scan of the subject's foot in resting pose). The sinking depth of the rigid foot was equal to the deepest part of the real moving foot at mid-stance. The timing was such that the indentation and removal of the rigid foot took the same number of frames as the experimental trial being simulated, i.e. the simulated time taken to 'stamp' the rigid foot was equal to the real timing of the original footstep. This most simplistic scenario was followed first by a single rigid foot rotating to approximate a heel–toe cycle, and then by a two-part foot in which the toes were able to rotate as an object independently of the foot (i.e. with a simple hinge at the approximate positions of the metatarsophalangeal joints). The single rotating foot object was animated to sink in the substrate such that the maximum depth of the metatarsal heads matched the depth of the metatarsal heads in the biplanar X-ray data. While this meant that the majority of the foot approximated the motion of the biplanar X-ray data, the toes necessarily sank much farther due to significant rotation. The two-part model alleviated this by allowing the toes to remain more horizontal as the heel lifted off the substrate. This two-part rigid-body simulation is analogous to previous footprint simulation work [22,28] in which individual toe segments were treated as separate translating and rotating rigid bodies.

However, these rigid-body models failed to capture subtle deformations of the human foot, particularly involving flexibility of the arches. Our final simulation used the animated high-resolution foot mesh directly, capturing as much of the reconstructed motion as possible. To do this, mesh face and vertex positions were output at a far greater temporal resolution; 1000 frames per second. LIGGGHTs input files ran 1000 time steps (each of 0.000001 s real time) between each frame to translate the mesh from one position to the next. This produced the most 'realistic' simulations, incorporating all motion of the deforming foot as

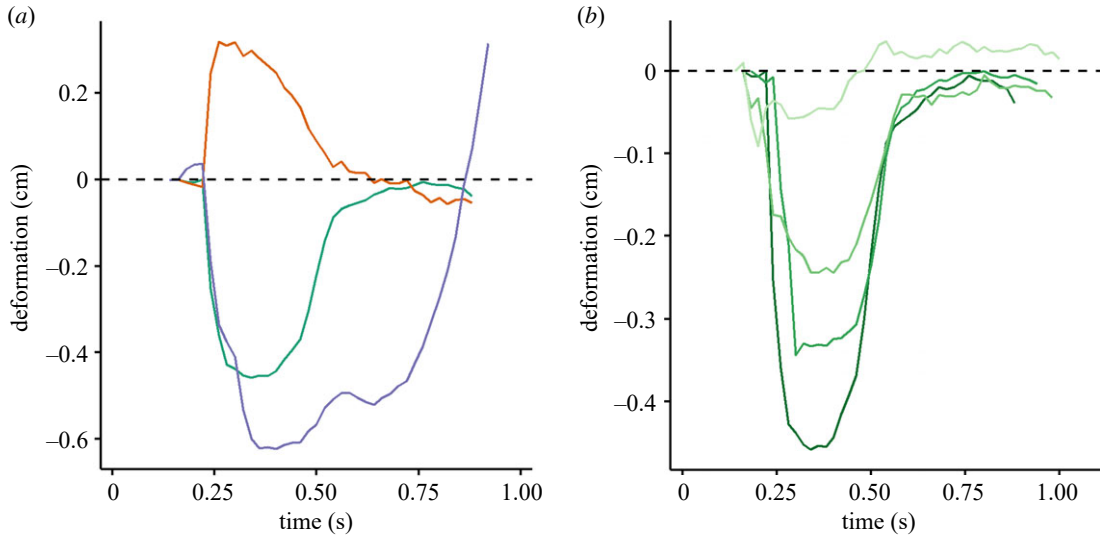

Figure 5. 3D deformation of the foot of one individual walking across multiple substrates. (*a*) Continuous measurements of heel height (green), heel width (orange) and medial longitudinal arch height (purple) during one trial on carbon fibre. Each measurement is zeroed based on its first possible measurement (prior to initial contact, when the foot first entered both biplanar X-ray video frames). (*b*) Sample plots showing deformation of the heel (change in vertical height) in one subject walking across four different substrates. Substrates become more deformable as they transition from darker to lighter shades of green (carbon fibre is the darkest green, 'firm' mud is the second darkest, 'hydrated 2.5' mud is the second lightest and 'hydrated 5' mud is the lightest).

derived from the skin markers placed on the subject. Simulations were visualized using OVITO (v. 3.0.0) [33].

3. Results and discussion

Using the methods described above, we successfully built data-driven 3D animations of deformable feet navigating deformable substrates to produce tracks (electronic supplementary material, video S1). Since the methodological developments are the focus of this paper, we present data from a single subject as a case study to demonstrate the variety of analyses that are permitted through the application of these novel methods.

The first area in which we can apply these techniques is to study 3D kinematics of the foot. The biplanar X-ray technique presented here provides a window for direct visualization of the foot–substrate interface while a human foot travels into, and interacts with, both rigid and deformable substrates. As in our prior studies [25], the 3D positions of external foot markers, visualized through biplanar X-ray, can be used to quantify 3D deformations of the plantar surface of the foot during its interactions with these various substrates. For example, continuous measurements of heel compression, heel expansion and longitudinal arch deformation can be collected throughout the duration of the stance phase to understand soft tissue behaviour in these regions of the foot (figure 5).

Figure 5 portrays temporal and substrate-driven patterns of foot deformation consistent with those previously observed by Hatala *et al*. [25]. The external surface of the heel simultaneously compressed vertically and expanded horizontally as the calcaneal fat pad dissipated impact forces (figure 5*a*), a pattern which has been well studied experimentally [34–36]. The medial longitudinal arch initially flattened as the foot was loaded, but at the terminal stance phase, it eventually reached a height that exceeded its initial, unloaded, state (figure 5*a*), consistent with results from other experimental studies of longitudinal arch function [37]. Comparisons across substrates likewise followed patterns observed previously by Hatala *et al*. [25]. For example, the heel compressed to greater degrees as subjects walked over more rigid substrates (figure 5*b*). Clearly, these are not the only types of dynamic measurements that can be acquired, and a variety of 3D kinematic studies would be possible through this approach. We simply emphasize here that our experimental protocol offers several directions to study foot–substrate interactions across rigid and deformable substrates using external marker-based kinematics.

Building upon studies of pure foot deformation and motion, the integration of high-resolution 3D models of both feet and tracks within the same animation scene provides opportunities to observe directly the extent and nature of the correspondence between external foot motions and the morphology of the final track that was produced. Previous studies have highlighted the lack of direct correspondence between foot motion and track morphology [25] and similar patterns were observed here. It is evident that final track morphology is not simply a Boolean-type subtraction of the foot's trajectory through the substrate. While the lack of correspondence between foot trajectories and final track morphology can be observed from the results of 3D animations of experimental trials, a true understanding of these differences requires knowledge of human track ontogeny. Such knowledge can be gained through track simulations, which allow one to visualize and understand the patterns of substrate flow that generate specific aspects of track morphology. Here, we explored as a case study a single trial from our biplanar X-ray experiments, in which a subject walked across 'hydrated 5' mud to produce a track. The 3D scan of that track was directly compared with simulated tracks that were produced following the track simulation protocols described above.

By iteratively increasing the complexity of the deformation and motion of the animated foot, we achieved simulations that eventually produced track morphologies that closely matched those produced in biplanar X-ray experiments (figure 6 and table 1). The simplest simulation, in which a rigid foot model vertically stamped a substrate, actually generated a track morphology with the smallest average pairwise distance from the 3D scanned track (table 1) and that looked qualitatively realistic. However, the similarities between the simulated and

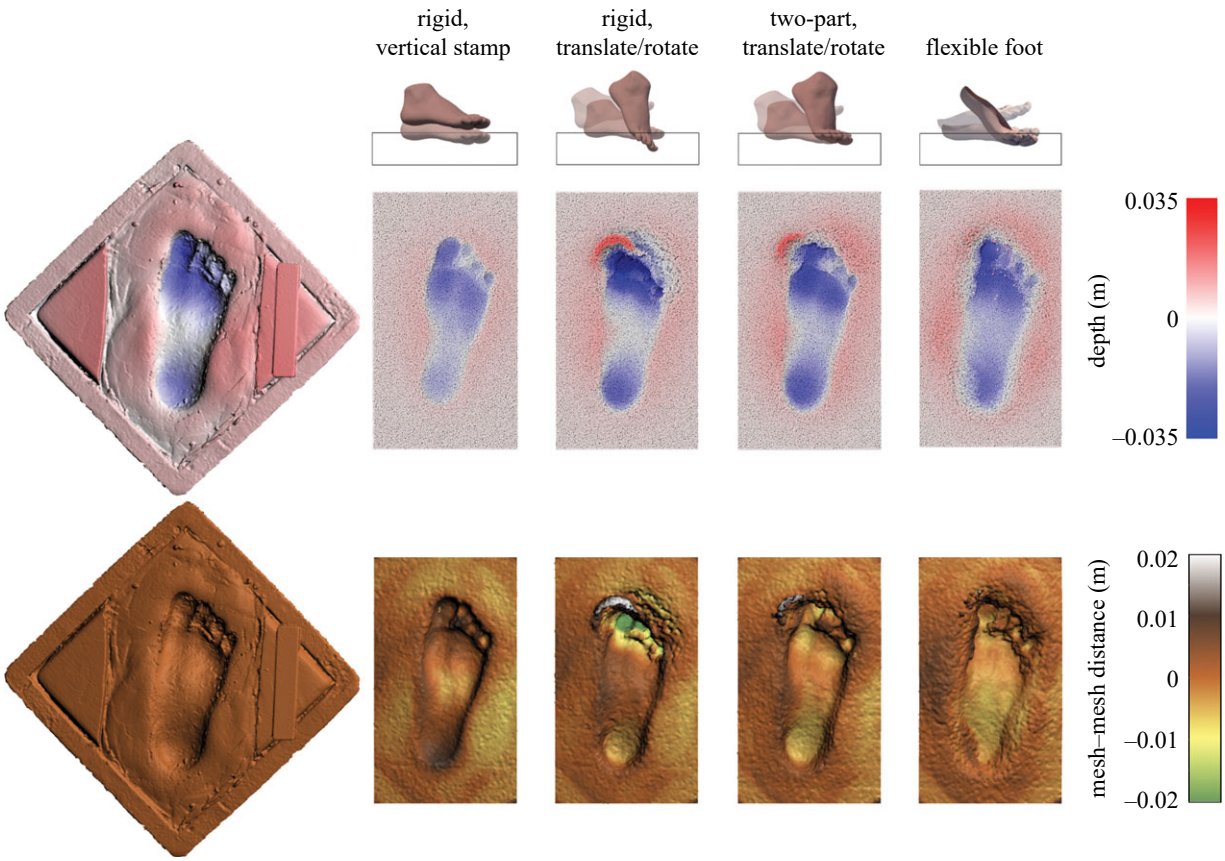

Figure 6. Direct comparisons between the 3D scan of track from biplanar X-ray experiments (left) and 3D meshes of tracks produced in various particle simulations (right). Simulations increase in complexity from left to right, from a vertical stamp of a rigid foot to a step taken by a fully flexible foot, whose motions and deformations were driven by real data from biplanar X-ray experiments. Top row shows track depths (in metres) as measured from the ground plane. Bottom row shows pairwise distances between each simulated track and the actual 3D scanned track. Differences between simulation conditions are subtle, but overall the most complicated animation/simulation converges on a track morphology that is most similar to the one actually produced in biplanar X-ray experiments.

Table 1. Summary statistics for pairwise distance comparisons between simulated tracks and 3D scanned track from biplanar X-ray experiments.

simulation type	mean distance (cm)	standard deviation (cm)
rigid foot, vertical stamp	0.0062	0.3446
rigid foot, translate/rotate	−0.0286	0.5980
two-part foot, translate/rotate	0.0556	0.3511
fully flexible animated foot	0.0176	0.2885

scanned tracks were largely confined to the region of the forefoot (figure 6). This was unsurprising, since the simulated foot trajectories were configured such that maximum depth beneath the metatarsal heads matched the depths to which the metatarsal heads were observed to travel in biplanar X-ray experiments (i.e. all simulations are most likely to match the 3D scanned track in the region of the forefoot). The 'vertical stamp' produced a track that was notably shallower and narrower than the scanned track in the region of the heel, and that had an overall less longitudinally arched shape. This track also lacked the displacement rims that surrounded the perimeter of the scanned track.

By adding motion to the rigid foot model (translating and rotating a rigid foot), we produced simulated tracks that had greater relative elevation beneath the longitudinal arch but that were otherwise quite different from the 3D scanned track. Toe impressions were extremely deep, the heel impression was deeper than observed in the scanned track, and a very notable extrusion feature was generated at the tip of the hallux (figure 6). Displacement rims were still not as prominent as they were in the 3D scanned experimental track. Adding a simple hinge to convert the rigid foot into a two-part model (allowing the foot to deform at the approximate positions of the metatarsophalangeal joints) remedied some but not all of these inaccuracies. Forefoot (including toe) impressions were overall more similar to those of the 3D scanned track, but the heel impression was still deeper and the extrusion feature at the tip of the hallux was still generated (figure 6).

Implementing a fully mobile and deformable foot animation led to simulated tracks that most closely matched those observed in biplanar X-ray experiments. The mean distance between the simulated and 3D scanned tracks was only the second lowest but the standard deviation was the smallest, indicating that this simulation varied the least of the four scenarios from the original scanned surface (table 1). The simulated track was similar in relative depths across the forefoot (including toe) impressions, in relative depths in the region of the heel and in the pattern of the displacement rim surrounding the perimeter of the track (figure 6). It was also the widest track in the mid-foot, which matched most closely with the real track. The simulated track had a slightly deeper impression beneath the longitudinal arch than did the 3D scanned track, but this difference was relatively subtle.

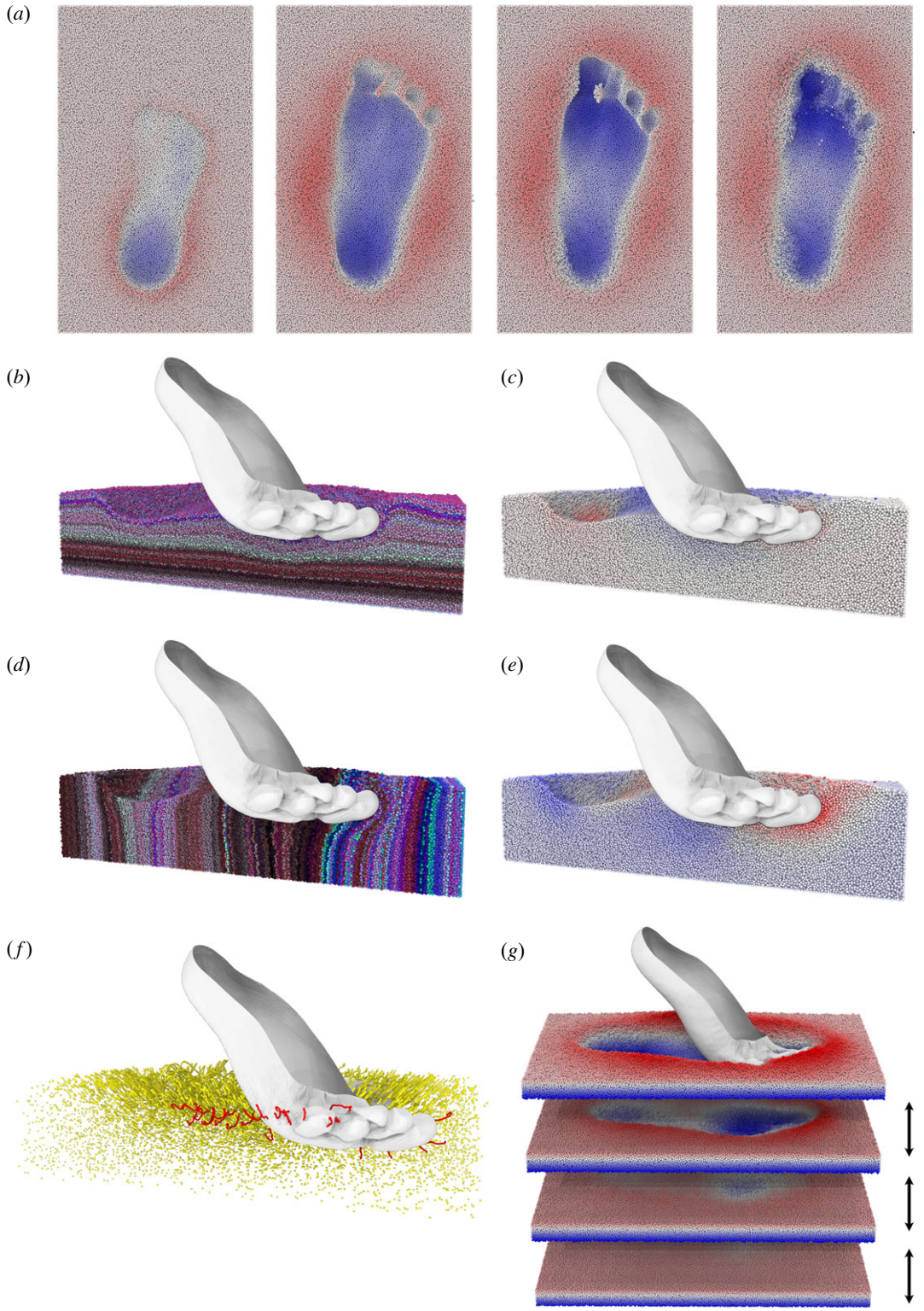

Figure 7. Examples of visualization methods applicable to our simulated tracks. (*a*) Track ontogenetic sequence at approximately 25%, 50%, 75% and 100% of stance phase. Colour scale indicates height, and difference between darkest blue and darkest red is 7 cm. (*b*) Randomized horizontal colouring, exposed through longitudinal section, provides a view comparable to observing a laminated sediment. (*c*) Medio-lateral motion of individual particles can be represented with colour, blue particles having moved medially, and red particles having moved laterally. (*d*,*e*) Visualization of forward/backward motion of particles as either randomized vertical coloration (*d*) or colour-coded such that red indicates forward motion, blue indicates backward motion (*e*). (*f*) Demonstration of particle vectors throughout the track formation process. Particles of interest, such as those in red which form the displacement rims, can be tracked separately and individually. (*g*) The simulated track can be split at virtual bedding planes, exposing a sequence of penetrative and transmitted undertracks.

It is clear from our simulated tracks that, as might be expected, incorporation of more complex motions and soft tissue deformations results in a more true-to-life final track morphology. That the real track differed substantially from the 'stamp' simulation demonstrates once again that 'footprints are not feet' and should not be interpreted as direct reflections of plantar foot anatomy [29]. Our simulated tracks also highlight caution in using simple metrics such as mean mesh–mesh distances to compare tracks; the complex 3D topography means that mean distances can be low, even when tracks are clearly qualitatively different.

Focusing on our most complex simulation (deformable foot), the qualitative and quantitative similarity between the simulated track and the real scanned track is gratifying, and indicates that the real motions of the foot and substrate are captured by our workflow. Minor differences between the final simulated track and the 3D scan of the real impression can be attributed to simulation parameters, particularly particle size and cohesion, though refining these parameters further would require substantial iterative simulations, which for the purposes of this study were deemed unnecessary. The nature of how the sediments are mixed and the set-up during the experimental protocol means that the bulk properties of the experimental substrate (particularly as it overlies elastically behaving foam) would be difficult to ascertain from a smaller, and thus easier to simulate, sample. As such, we base our input parameters on what makes the output most like the scanned track, but as elaborated on previously [28] significant deviations between simulation and reality would indicate that our input parameters are incorrect. We, therefore, consider our simulation, based on its qualitative and quantitative similarity to the scanned track, to accurately represent the pattern of surface and subsurface substrate deformation that occurred during the biplanar X-ray experiment.

Armed with this complete simulation of animated, deforming foot morphology and a deformable substrate responding to that foot, we are able to visualize and explore the formation of the track—its ontogeny—in a multitude of ways at and beneath the sediment surface (figure 7). Examining a sequence of time steps during the foot–substrate interaction allows us to visualize the temporal process of track development (figure 7*a*). Using randomized bands of colour oriented either vertically or horizontally enables visualization of the directions and magnitudes of particle motion within the substrate (figure 7*b*,*d*). Colour gradients can also be applied to individual particles, in order to visualize how far they move in various directions (figure 7*c*,*e*). Particle trajectories can be traced in order to track the motions of individual particles or groups of particles within the substrate throughout the track formation process (figure 7*f*). For instance, selecting particles in the displacement rims and generating trajectories backwards, we can identify where the raised sediment has been pushed from. Subsurface layers can be exposed, presenting transmitted undertracks (figure 7*g*). Ultimately there are countless directions that one can pursue to visualize track ontogeny, and understand how various aspects of track morphology were generated. We do not exhaustively list the possibilities here, but merely emphasize a variety of visualization techniques that can reveal previously hidden aspects of the track formation process.

4. Conclusion

The combination of biplanar X-ray, 3D animation and particle simulation methods that we have introduced and applied here have the potential to inform a wide variety of research questions related to how locomotion varies across substrates with different mechanical properties, and how tracks can record those variations. Instruments that are ubiquitous to biomechanics laboratories, such as force plates, pressure pads and optical motion capture systems, provide richly detailed understandings of how our feet function during locomotion. However, force- and pressure-sensing instruments are typically rigid and the opacity of feet and substrates conceals the interactions that occur at the foot–substrate interface, so these instruments are for the most part limited to studying locomotion on rigid surfaces. The hidden interactions between the foot and deformable substrate are of interest to researchers across many disciplines that seek to better understand their mechanics. For example, in biorobotics, a great deal of attention has been devoted to understanding how animals traverse irregular, deformable terrain. It has been challenging to build robots that can navigate natural environments and their inherent unpredictability, in part due to limited abilities to observe and measure mechanical interactions at the foot–substrate interface [38,39]. In human biomechanics, understandings of locomotion and foot function across non-rigid substrates are similarly limited. It is known that humans alter their kinematics on deformable substrates, and that the energetic costs of locomotion increase with substrate compliance [40–42]. However, it has been exceedingly difficult to observe and quantify the manners in which human feet engage with non-rigid substrates. The methods described here are transferable to these and other systems, and have the potential to open windows on previously unobservable biomechanical phenomena. This emphasizes the interdisciplinarity that is inherent to these approaches.

Within palaeoanthropology, the methods developed here substantially expand the toolkit that can be applied to analyse hominin tracks. Previous experimental studies, including our own, have relied on the comparative method to determine whether and how various hominin tracks differ from each other, and to develop anatomical and/or functional hypotheses for those differences [9,11,43–48]. The methods presented here focus instead on building knowledge of human track ontogeny, in order to understand how particular anatomical or functional patterns lead to the development of specific track morphologies. Through validated track simulation methods, the combinations of foot anatomy and motion that would be capable of producing particular fossil track morphologies can be reverse-engineered [28]. When synthesized with 'functional' analyses of skeletal fossils (e.g. analyses of trabecular bone, cross-sectional geometry and/or articular morphology), these simulation-based analyses of fossil hominin tracks provide an unparalleled route to explicitly test and develop hypotheses regarding fossil hominin locomotion.

Ethics. Experiments with human subjects included only participants who provided their informed consent to participate, in accordance with protocols jointly approved by the Institutional Review Boards of Brown University and Chatham University.

Data accessibility. All data and code required to replicate the findings presented here have been made publicly available (doi:10.6084/m9.figshare.13090367).

Authors' contributions. All authors contributed to the conception and design of the project. K.G.H. and S.M.G. carried out biplanar X-ray experiments, with input from P.L.F. P.L.F. carried out substrate simulations, with input from K.G.H. and S.M.G. All authors collaboratively drafted and edited the manuscript, and all agree to be accountable for the work presented here.

Competing interests. We declare we have no competing interests.

Funding. This work was supported by the National Science Foundation (BCS-1825403 to K.G.H. and P.L.F.; and BCS-1824821 to S.M.G.) and Chatham University.

Acknowledgements. We thank Michael Berthaume and Patricia Kramer for their invitation to contribute to this special issue. We thank David Baier, Beth Brainerd, Spencer Cheleden, Kay Fiske, Kia Huffman, Ben Knörlein, David Laidlaw, Kyra Tani Little, Armita

Manafzadeh, Sabreen Megherhi, Johannes Novotny, David North and Morgan Turner for assistance directly related to the design and implementation of this project. We also thank the anonymous volunteers who participated in these experiments.

References

1. Darwin C. 1871 *The descent of man, and selection in relation to sex.* London, UK: John Murray.
2. DeSilva J, McNutt E, Benoit J, Zipfel B. 2019 One small step: a review of Plio-Pleistocene hominin foot evolution. *Am. J. Phys. Anthropol.* **168**, 63–140. (doi:10.1002/ajpa.23750)
3. Day MH, Napier JR. 1964 Fossil foot bones. *Nature* **201**, 969–970. (doi:10.1038/201969a0)
4. Jungers WL, Harcourt-Smith WEH, Wunderlich RE, Tocheri MW, Larson SG, Sutikna T, Due RA, Morwood MJ. 2009 The foot of *Homo floresiensis*. *Nature* **459**, 81–84. (doi:10.1038/nature07989)
5. Harcourt-Smith WEH *et al.* 2015 The foot of *Homo naledi*. *Nat. Commun.* **6**, 8432. (doi:10.1038/ncomms9432)
6. DeSilva JM, Gill CM, Prang TC, Bredella MA, Alemseged Z. 2018 A nearly complete foot from Dikika, Ethiopia and its implications for the ontogeny and function of *Australopithecus afarensis*. *Sci. Adv.* **4**, eaar7723. (doi:10.1126/sciadv.aar7723)
7. Gatesy SM, Middleton KM, Jenkins Jr FA, Shubin NH. 1999 Three-dimensional preservation of foot movements in Triassic theropod dinosaurs. *Nature* **399**, 141–144. (doi:10.1038/20167)
8. Manafzadeh AR, Padian K. 2018 ROM mapping of ligamentous constraints on avian hip mobility: implications for extinct ornithodirans. *Proc. R. Soc. B* **285**, 20180727. (doi:10.1098/rspb.2018.0727)
9. Bennett MR *et al.* 2009 Early hominin foot morphology based on 1.5-million-year-old footprints from Ileret, Kenya. *Science* **323**, 1197–1201. (doi:10.1126/science.1168132)
10. Ashton N *et al.* 2014 Hominin footprints from early Pleistocene deposits at Happisburgh, UK. *PLoS ONE* **9**, e88329. (doi:10.1371/journal.pone.0088329)
11. Hatala KG *et al.* 2016 Footprints reveal direct evidence of group behavior and locomotion in *Homo erectus*. *Sci. Rep.* **6**, 28766. (doi:10.1038/srep28766)
12. Hatala KG *et al.* 2017 Hominin track assemblages from Okote Member deposits near Ileret, Kenya, and their implications for understanding fossil hominin paleobiology at 1.5 Ma. *J. Hum. Evol.* **112**, 93–104. (doi:10.1016/j.jhevol.2017.08.013)
13. Masao FT, Ichumbaki EB, Cherin M, Barili A, Boschian G, Iurino DA, Menconero S, Moggi-Cecchi J, Manzi G. 2016 New footprints from Laetoli (Tanzania) provide evidence for marked body size variation in early hominins. *eLife* **5**, 29. (doi:10.7554/eLife.19568)
14. Altamura F *et al.* 2018 Archaeology and ichnology at Gombore II-2, Melka Kunture, Ethiopia: everyday life of a mixed-age hominin group 700,000 years ago. *Sci. Rep.* **8**, 1–11. (doi:10.1038/s41598-018-21158-7)
15. Altamura F, Bennett MR, Marchetti L, Melis RT, Reynolds SC, Mussi M. 2020 Ichnological and archaeological evidence from Gombore II OAM, Melka Kunture, Ethiopia: an integrated approach to reconstruct local environments and biological presences between 1.2 and 0.85 Ma. *Quat. Sci. Rev.* **244**, 106506. (doi:10.1016/j.quascirev.2020.106506)
16. Bennett MR, Falkingham P, Morse SA, Bates K, Crompton RH. 2013 Preserving the impossible: conservation of soft-sediment hominin footprint sites and strategies for three-dimensional digital data capture. *PLoS ONE* **8**, e60755. (doi:10.1371/journal.pone.0060755)
17. Falkingham PL *et al.* 2018 A standard protocol for documenting modern and fossil ichnological data. *Palaeontology* **61**, 469–480 (doi:10.1111/pala.12373)
18. Minter NJ, Braddy SJ, Davis RB. 2007 Between a rock and a hard place: arthropod trackways and ichnotaxonomy. *Lethaia* **40**, 365–375. (doi:10.1111/j.1502-3931.2007.00035.x)
19. Padian K, Olsen PE. 1984 The fossil trackway *Pteraichnus*: not pterosaurian, but crocodilian. *J. Paleontol.* **58**, 178–184. (https://www.jstor.org/stable/1304743)
20. Falkingham PL. 2014 Interpreting ecology and behaviour from the vertebrate fossil track record. *J. Zool.* **292**, 222–228. (doi:10.1111/jzo.12110)
21. Morse SA, Bennett MR, Liutkus-Pierce C, Thackeray JF, McClymont J, Savage R, Crompton RH. 2013 Holocene footprints in Namibia: the influence of substrate on footprint variability. *Am. J. Phys. Anthropol.* **151**, 265–279. (doi:10.1002/ajpa.22276)
22. Falkingham PL, Gatesy SM. 2014 The birth of a dinosaur footprint: subsurface 3D motion reconstruction and discrete element simulation reveal track ontogeny. *Proc. Natl Acad. Sci. USA* **111**, 18 279–18 284. (doi:10.1073/pnas.1416252111)
23. Maladen R, Ding Y, Li C, Goldman DI. 2009 Undulatory swimming in sand: subsurface locomotion of the sandfish lizard. *Science* **325**, 314–318. (doi:10.1126/science.1172490)
24. Ellis RG, Gatesy SM. 2013 A biplanar X-ray method for three-dimensional analysis of track formation. *Palaeontol. Electron.* **16**, 16.1.1T. (doi:10.26879/324)
25. Hatala KG, Perry DA, Gatesy SM. 2018 A biplanar X-ray approach for studying the 3D dynamics of human track formation. *J. Hum. Evol.* **121**, 104–118. (doi:10.1016/j.jhevol.2018.03.006)
26. Cundall PA, Strack ODL. 1979 A discrete numerical model for granular assemblies. *Géotechnique* **29**, 47–65. (doi:10.1680/geot.1979.29.1.47)
27. Kloss C, Goniva C. 2011 LIGGGHTS—open source discrete element simulations of granular materials based on Lammps. In *TMS2011, 140th Annual Meeting & Exhibition, San Diego, CA, 27 February–3 March, Suppl. Proc., Vol. 2, Materials fabrication, properties, characterization, and modeling* (ed. Minerals, Metals & Materials Society), pp. 781–788. Hoboken, NJ: John Wiley. (doi:10.1002/9781118062142.ch94)
28. Falkingham PL, Turner ML, Gatesy SM. 2020 Constructing and testing hypotheses of dinosaur foot motions from fossil tracks using digitization and simulation. *Palaeontology* **63**, 865–880. (doi:10.1111/pala.12502)
29. Gatesy SM, Falkingham PL. 2017 Neither bones nor feet: track morphological variation and 'preservation quality.' *J. Vertebr. Paleontol.* **37**, e1314298. (doi:10.1080/02724634.2017.1314298)
30. Brainerd EL *et al.* 2010 X-ray Reconstruction of Moving Morphology (XROMM): precision, accuracy and applications in comparative biomechanics research. *J. Exp. Zool. A* **313**, 262–279. (doi:10.1002/jez.589)
31. Knörlein BJ, Baier DB, Gatesy SM, Laurence-Chasen JD, Brainerd EL. 2016 Validation of XMALab software for marker-based XROMM. *J. Exp. Biol.* **219**, 3701–3711. (doi:10.1242/jeb.145383)
32. Baier DB. 2018 XROMM Maya Tools. See https://bitbucket.org/xromm/xromm_mayatools/src/master/.
33. Stukowski A. 2010 Visualization and analysis of atomistic simulation data with OVITO—the Open Visualization Tool. *Model. Simul. Mater. Sci. Eng.* **18**, 015012. (doi:10.1088/0965-0393/18/1/015012)
34. De Clercq D, Aerts P, Kunnen M. 1994 The mechanical characteristics of the human heel pad during foot strike in running: an *in vivo* cineradiographic study. *J. Biomech.* **27**, 1213–1222. (doi:10.1016/0021-9290(94)90275-5)
35. Gefen A, Megido-Ravid M, Itzchak Y. 2001 *In vivo* biomechanical behavior of the human heel pad during the stance phase of gait. *J. Biomech.* **34**, 1661–1665. (doi:10.1016/S0021-9290(01)00143-9)
36. Chi KJ, Schmitt D. 2005 Mechanical energy and effective foot mass during impact loading of walking and running. *J. Biomech.* **38**, 1387–1395. (doi:10.1016/j.jbiomech.2004.06.020)
37. Caravaggi P, Pataky T, Gunther M, Savage R, Crompton R. 2010 Dynamics of longitudinal arch support in relation to walking speed: contribution of the plantar aponeurosis. *J. Anat.* **217**, 254–261. (doi:10.1111/j.1469-7580.2010.01261.x)
38. Ijspeert AJ. 2014 Biorobotics: using robots to emulate and investigate agile locomotion. *Science* **346**, 196–203. (doi:10.1126/science.1254486)
39. Aguilar J *et al.* 2016 A review on locomotion robophysics: the study of movement at the intersection of robotics, soft matter and dynamical systems. *Rep. Prog. Phys.* **79**, 110001. (doi:10.1088/0034-4885/79/11/110001)

40. Ferris DP, Louie M, Farley CT. 1998 Running in the real world: adjusting leg stiffness for different surfaces. *Proc. R. Soc. B* **265**, 989–994. (doi:10.1098/rspb.1998.0388)
41. Lejeune TM, Willems PA, Heglund NC. 1998 Mechanics and energetics of human locomotion on sand. *J. Exp. Biol.* **201**, 2071–2080. (doi:10.1242/jeb.201.13.2071)
42. Kerdok AE, Biewener AA, McMahon TA, Weyand PG, Herr HM. 2002 Energetics and mechanics of human running on surfaces of different stiffnesses. *J. Appl. Physiol.* **92**, 469–478. (doi:10.1152/japplphysiol.01164.2000)
43. Day MH, Wickens EH. 1980 Laetoli Pliocene hominid footprints and bipedalism. *Nature* **286**, 385–387. (doi:10.1038/286385a0)
44. Tuttle RH, Webb DM, Weidl E, Baksh M. 1990 Further progress on the Laetoli trails. *J. Archaeol. Sci.* **17**, 347–362. (doi:10.1016/0305-4403(90)90028-4)
45. Meldrum DJ, Wunderlich RE. 1998 Midtarsal flexibility in ape foot dynamics, early hominid footprints and bipedalism. *Am. J. Phys. Anthropol. Suppl.* **26**, 161.
46. Raichlen DA, Gordon AD, Harcourt-Smith WEH, Foster AD, Haas WR. 2010 Laetoli footprints preserve earliest direct evidence of human-like bipedal biomechanics. *PLoS ONE* **5**, e9769. (doi:10.1371/journal.pone.0009769)
47. Crompton RH, Pataky TC, Savage R, D'Août K, Bennett MR, Day MH, Bates K, Morse S, Sellers WI. 2012 Human-like external function of the foot, and fully upright gait, confirmed in the 3.66 million year old Laetoli hominin footprints by topographic statistics, experimental footprint-formation and computer simulation. *J. R. Soc. Interface* **9**, 707–719. (doi:10.1098/rsif.2011.0258)
48. Hatala KG, Demes B, Richmond BG. 2016 Laetoli footprints reveal bipedal gait biomechanics different from those of modern humans and chimpanzees. *Proc. R. Soc. B* **283**, 20160235. (doi:10.1098/rspb.2016.0235)